LIDAR SEGMENTATION USING SUITABLE SEED POINTS FOR 3D BUILDING EXTRACTION

S M Abdullah[1], Mohammad Awrangjeb[2] and Guojun Lu[2]

[1] Faculty of Information Technology, Monash University, Clayton, VIC-3800, Australia
[2] School of Information Technology, Federation University Australia, Churchill, VIC-3842, Australia
[1] sm.abdullah@monash.edu, [2] {mohammad.awrangjeb,guojun.lu}@federation.edu.au

KEY WORDS: LiDAR data, segmentation, seed point, building detection, roof plane extraction, tree removal

ABSTRACT:

Effective building detection and roof reconstruction has an influential demand over the remote sensing research community. In this paper, we present a new automatic LiDAR point cloud segmentation method using suitable seed points for building detection and roof plane extraction. Firstly, the LiDAR point cloud is separated into "ground" and "non-ground" points based on the analysis of DEM with a height threshold. Each of the non-ground point is marked as coplanar or non-coplanar based on a coplanarity analysis. Commencing from the maximum LiDAR point height towards the minimum, all the LiDAR points on each height level are extracted and separated into several groups based on 2D distance. From each group, lines are extracted and a coplanar point which is the nearest to the midpoint of each line is considered as a seed point. This seed point and its neighbouring points are utilised to generate the plane equation. The plane is grown in a region growing fashion until no new points can be added. A robust rule-based tree removal method is applied subsequently to remove planar segments on trees. Four different rules are applied in this method. Finally, the boundary of each object is extracted from the segmented LiDAR point cloud. The method is evaluated with six different data sets consisting hilly and densely vegetated areas. The experimental results indicate that the proposed method offers a high building detection and roof plane extraction rates while compared to a recently proposed method.

1. INTRODUCTION

Among all of the artificial objects, buildings play a vital role in modern civilisation. From early civilisation till today its importance never changes. Hence it gains popularity among the remote sensing researchers to design and develop approaches for automatic building detection and roof plane extraction, which is an active research issue for more than two decades (Khoshelham and Li, 2005, Chenga et al., 2013). Accurate detection of building boundary and extraction of the individual roof plane can be a vital source of information for various applications, including urban planning, virtual reality, disaster management, detection of unlawful extension of properties, security, telecommunication and so on (Habib et al., 2010, Kabolizade et al., 2012). As a consequence, many different research activities have been conducted in this field. These can be split into three major groups (Awrangjeb and Fraser, 2013, Khoshelham and Li, 2005): *building detection*, *roof plane extraction*, and *roof/building reconstruction*. In this paper, we have concentrated with building detection and roof plane extraction.

Building detection is the process of identifying and subsequently separating the boundary of each building. The detection process becomes harder in the presence of vegetation and other non-building objects. More often than not, the process is utilised over a data set consisting of many buildings. The detected boundary can be optionally regularised to smooth the boundary. Many researchers employ the detection output to generate building footprint (Zhang et al., 2006).

Roof plane extraction is the process to identify individual roof planes. This process is similar to building detection. However, there is a subtle difference between them. Building detection process detects the individual building boundary, where the extraction process identifies each roof plane on a building. The process becomes more challenging with complex and small size roof planes.

The building detection and roof plane extraction process can be performed separately. However, some researchers (Awrangjeb et al., 2013) combined these two steps into one. We adopt the second approach. Our proposed method extracts individual roof planes and logically combines them in a neighbourhood basis to detect each building.

Building detection and roof plane extraction algorithms can be divided into three major groups based on input (Awrangjeb et al., 2012). They are: (a) image-based, (b) LiDAR-based, and (c) combination of imagery and LiDAR.

Many researchers have applied 2D or 3D information from the photogrammetric imagery for building detection and roof plane extraction (Noronha and Nevatia, 2001, Ferro et al., 2013). Different image cues such as NDVI and colour along with entropy can be applied for this purpose. Researchers have employed either satellite imagery (Ferro et al., 2013) or aerial imagery (Noronha and Nevatia, 2001) to attain this. Aerial imagery is more popular than satellite imagery for its higher spatial resolution. Image-based approaches suffer from various problems. A high resolution image contains more detail information, so the complexity of detecting buildings from the non-building objects increases as the resolution of the image increases (Cheng et al., 2008). Shadows and occlusions from nearby buildings and trees have also negative effect for building detection and roof extraction (Meng et al., 2009). The 3D information derived from stereo images, like depth information, is even more challenging (Vu et al., 2009) and offers poor accuracy. Moreover, the images contain several information and in many cases extraction of the required information is complex (Ferro et al., 2013).

In LiDAR (Light Detection And Ranging) based approaches, LiDAR point cloud is used for building detection and extraction. LiDAR is a remote sensing technology that measures the properties of scattered or reflected light to find distance and/or other information of a distant target (Carter et al., 2012). The current Li-

DAR point cloud is dense; it has high accuracy in height and can be used directly to extract the 3D objects on the earth. Unlike image acquisition systems, LiDAR data come from active systems, so LiDAR data can be gathered during the day or night (Elaksher and Bethel, 2002). The acquisition systems have other advantages like, fast data acquisition, high point density, and canopy penetration (Satari. et al., 2012).

Currently, many researchers are trying to combine high resolution imagery and LiDAR data for building detection and roof extraction (Awrangjeb et al., 2012). However, this process may fail to produce good quality results in some cases. Accurate co-registration of imagery and LiDAR data is a prerequisite for this approach. In many cases good quality data may not be available. If data acquisition is done at different times and if the time gap is higher, both data may not be same. In a densely vegetate area, most of the buildings are occluded by nearby trees. From imagery, buildings may not be detectable due to shadows and occlusions.

So considering the aforementioned issues, in this paper we have focused on the building detection and roof plane extraction process based on LiDAR data.

The rest of the paper is designed as follows: Section 2 discusses related research work for building detection and roof plane extraction using LiDAR data. Section 3 presents our contribution in the proposed method. Section 4 describes the proposed method, followed by the experimental results, analysis, and comparison in Section 5 and 6, respectively. Concluding remarks are provided in Section 7.

2. RELATED WORK

Different approaches for building detection and roof plane extraction using LiDAR data have been reported in the last few years. Many researchers use raw LiDAR data (Awrangjeb and Fraser, 2013), while others pre-processed it (Ma, 2005). Some authors initially classify the LiDAR data into several classes and employed only the required class (Chenga et al., 2013), while others segment the LiDAR data to extract ground and non-ground points (Awrangjeb et al., 2012). In this section, we will briefly describe some of the research work which is based on LiDAR data.

A rule-based segmentation algorithm was proposed in (Awrangjeb and Fraser, 2013). The proposed algorithm was based on 3D information from the LiDAR point cloud. The raw LiDAR data were initially divided into two groups based on a height threshold. The LiDAR points which had smaller heights than the threshold were used to generate a building mask. The remaining points were marked as non-ground points. These points were further classified based on the coplanarity of the points. The building mask was divided into cells. Based on the similarity, the cells were clustered and three different types of clusters were extracted. Using the coplanarity and neighbourhood information each of the planar roof segments was extracted. Finally, a rule-based approach was used to remove planar segments on trees. Experimental results showed that the approach missed small roof planes and buildings.

Sampath and Shan (Sampath and Shan, 2010) provided a solution framework for the segmentation of the LiDAR data. This method used the eigenanalysis of each LiDAR point to determine its planarity. Only the planar points were further considered for roof segmentation. For this purpose, the framework used a modified fuzzy *k*-means algorithm. The clustering algorithm is computationally expensive. Moreover the initial planar and non-planar separation of LiDAR points can lead to erroneous results as the surface normal becomes noisy for high point density (Novacheva, 2008). Experimental results showed that the framework provided better evaluation results for large roof planes. However, for small roof planes the results were not convincing.

A three step building detection technique have been proposed by Wang and Shan (Wang and Shan, 2009). At first, it identified the boundary and non-boundary points. These points were known as *jump edge points* and *crease edge points* respectively. By using the convex hull with nearest neighbourhood-based computation, the LiDAR points were labelled as boundary or non-boundary points. The boundary points were connected using *k-nearest* neighbour network and Minimum Spanning Tree (MST) to form the *jump edge*. For tree removal, the authors assumed that trees and buildings were separately enclosed by the different jump edges. It applied the dimensionality learning method to separate those. No quantitative results were presented in the paper.

Among other methods, some authors used morphological filtering and its variations (Meng et al., 2009, Chenga et al., 2013). A reverse iterative morphological algorithm was proposed in (Chenga et al., 2013). This method applied the morphological opening operation with gradually reduced window size. The algorithm separated the LiDAR points into buildings, trees, and other classes. It had some predefined data set specific thresholds for setting the maximum, the minimum window size and the minimum non-ground object height. A post-processing step with roughness and area information was used to remove non-building LiDAR points. However, the algorithm was tested only with 10 buildings where the minimum building size was over 500 m^2. It is unclear from the paper, whether the algorithm can be applicable for small buildings.

3. OUR CONTRIBUTION

The proposed method addresses some problems of a previously proposed method (Awrangjeb et al., 2013) and contributes to solve those problems. This section discusses two major problems of the previous method and provides a brief description how to solve them.

3.1 Problems of Using Mask

The previously proposed method generated two masks – primary and secondary mask from the LiDAR data utilising DEM with a height threshold. These masks were further used in the segmentation process. However, the generated masks missed some of the transparent roof top building objects. Figure 1 shows an orthoimage and its associated primary mask and highlights the missing objects.

As these buildings are missed in the mask generation step, this method could not extract them. Considering this problem, our proposed method does not depend on mask generation. It divides the LiDAR data into two sets based on a height threshold. LiDAR points on transparent rooftop are collected for segmentation and successfully extracted.

3.2 Issues Related to Image Lines

For roof plane extraction, the previously proposed method extracted lines from image and classified them as ‘ground’, ‘trees’, ‘roof ridge’, and ‘roof edge’. From the last two classified line sets, this method used a region growing approach to extract each roof segment. The image lines were used to identify seed points

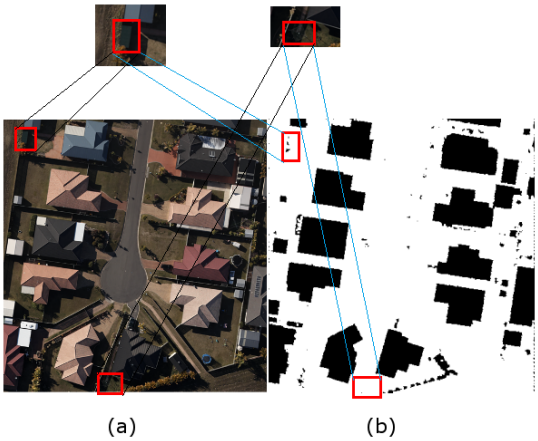

Figure 1: (a) Orthoimage; (b) Primary mask. Missing buildings of the reference method are marked by red coloured region in both images.

to grow the segment. However, if the image lines are missing, planes are missing too. Moreover, this method missed small buildings and small roof planes as it removed lines shorter than 1 m. Our proposed method solves this problem by coplanarity analysis and successfully includes small buildings and roof planes.

4. PROPOSED METHOD

The flow diagram in Figure 2 outlines the basic steps of the propose method.

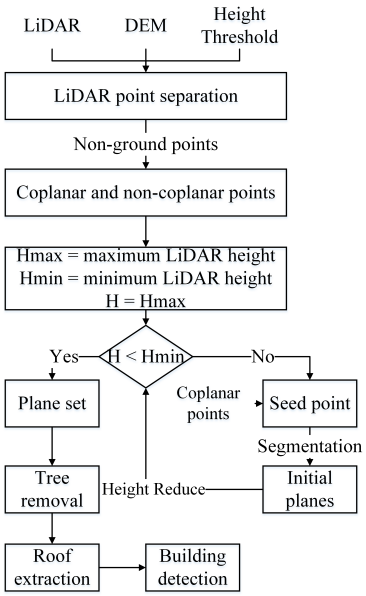

Figure 2: Flow diagram of the proposed method.

The proposed method commences with the LiDAR point cloud as input. Firstly, it divides the LiDAR point cloud into two sets, namely: ground and non-ground points. The elevation information from the DEM with a height threshold is used to separate the LiDAR point cloud. Secondly, each of the non-ground LiDAR point is marked as coplanar or non-coplanar based on a coplanarity analysis. The height level of the LiDAR data is reduced iteratively from the maximum to the minimum height and at each height level all the non-ground LiDAR points are collected. The collected points are divided into several groups based on 2D Euclidian distance. From each group, a coplanar point is selected as a seed point and the plane is grown in a region growing fashion until no new points can be added. A rule-based tree removal procedure is applied to remove planar segments on trees. Finally, the planar segments are combined on a neighbourhood basis to obtain individual building boundaries.

4.1 LiDAR Point Separation

Morgan (Morgan, 2000) showed classifying ground and non-ground points is a critical step for segmenting LiDAR data. Hence different approaches were reported in the literature to divide or classify the LiDAR point cloud. We are using elevation information from the DEM to divide the LiDAR point cloud into ground and non-ground points. The DEM has been generated from the input LiDAR point cloud by using the commercial software MARS Explorer (MARS Explorer version 7, 2014). The process iteratively selects each LiDAR point and takes ground height from the DEM. A LiDAR point is considered as a non-ground point if it is at least 1 m (Awrangjeb and Fraser, 2013) above the ground height. The minimum object height of 1 m is chosen carefully, hence we can detect low height buildings. Though many authors used different threshold values such as 2 m (Zhang et al., 2006) or 2.5 m (Awrangjeb et al., 2012) or even higher to minimize the effect of the bushes and small vegetation, but they were unable to detect low height buildings. From now on LiDAR point cloud refers in this paper contains only the non-ground points.

4.2 Coplanar and Non-coplanar Point

In this section, LiDAR points are classified as coplanar and non-coplanar points. The coplanar points will be used to determine seed points. The idea of classifying the LiDAR points as coplanar and non-coplanar is adopted from (Sampath and Shan, 2010). The eigenvalues of the covariance matrix are used to ascertain whether a point is coplanar or non-coplanar. The eigenvalues $(\lambda_1, \lambda_2, \lambda_3$ where $\lambda_1 \leq \lambda_2 \leq \lambda_3)$ imply the dimensionality of the LiDAR point. If the dimensionality is two, there would exist only two nonzero eigenvalues. If the dimensionality of the point is three, all the three eigenvalues will be zero. However, due to inherent noise of LiDAR data it is not reasonable to expect zero eigenvalues even for a coplanar neighbourhood. A normalised eigenvalue is considered instead of using individual eigenvalues. If it is at least 0.005 (Sampath and Shan, 2010) the point is considered as coplanar along with its neighbourhood. The neighbourhood of each point is determined using 2D Delaunay triangulation.

Figure 3 shows the coplanar and non-coplanar LiDAR points for a data set. The points which are marked by yellow colour are the coplanar points and the remaining are non-coplanar. As can be seen from this figure, the majority of the points on trees are non-coplanar and those on buildings are coplanar.

4.3 Seed Point Selection

The process starts with the maximum LiDAR point height, accumulating all of the points at each height level with a tolerance height threshold. This can be represented as $M = \{p \in P | h_l - \tau < h_p <= h_l + \tau\}$, here P represents the LiDAR point cloud where h_p represents the height of point p and h_l corresponds the current height level. Points satisfying the above equation are selected where τ indicates the tolerance height threshold, which is set 10 cm. Though dense LiDAR data provide high accuracy in height, but it has inherent noise. Hence, on a particular height level all the LiDAR points do not have the similar height,

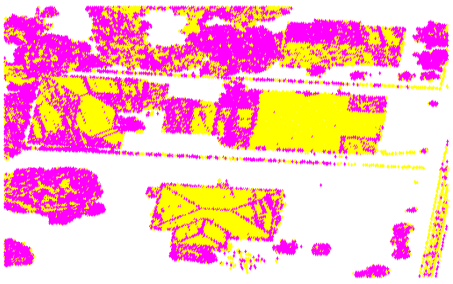

Figure 3: Coplanar and non-coplanar points for a data set: coplanar (yellow dots) and non-coplanar (magenta dots) LiDAR points.

although they can be fitted into a planar surface. Since the error in the LiDAR estimated height is usually higher than 10 cm, (Liu, 2011) $\tau = 10$ cm is a reasonable threshold. All of the points in M may not belong to the same building or plane. The points in M are clustered based on 2D Euclidian distance. Each of the clusters is used to extract lines. These extracted lines are used to select the best suitable seed point for a plane. A coplanar point which is the nearest to the midpoint of each line is considered as the seed point. The aforementioned process runs iteratively and in each step h_l is reduced by 0.5 m until it reaches the minimum LiDAR point height. This height reduction threshold is set empirically. If the density of the LiDAR point cloud is low ($<= 1$ point/m^2), then the chance of getting new seed points for plane extraction will be eventually low. However, for high density point cloud the possibility increases. Setting the value as 0.5 m allows us not to lose any significant plane, even at a low point density.

4.4 Plane Extraction

The seed point and its neighbouring points are used to generate the initial plane equation. The neighbourhood is determined by the 2D Euclidian distance from the seed point. The seed point and its neighbouring points are used to determine the plane equation. The initial plane is growing in a region grown fashion until no new points can be added. To grow the initial plane, those points are chosen which are the neighbourhood of the current plane but do not belongs to it. Before updating the plane equation, the new points are judged based on a plane fitting error and the height difference between the estimated height and the LiDAR point height of the points. Two different thresholds were proposed in (Awrangjeb et al., 2013) for this purpose. All the new points which satisfy one of the two threshold values are added to the initial plane and the coefficients of the plane equation are updated.

By using raw LiDAR data, the possibilities of extracting non-building planes are higher. To reduce this effect, the average standard deviation of height of all of the non-ground LiDAR points is used. Comparatively, planes on trees have a higher standard deviation of height than planes on buildings. To evaluate this observation, we calculated the standard deviation of height of all the extracted planes along with an average standard deviation. The calculated result supports our observation. Figure 4 shows the effect of standard deviation of height.

It is clear from the figure that the buildings have lower standard deviation of height. The observation helps us to remove some of the trees in the detection process. Figure 5 illustrates all of the extracted initial planar segments after plane extraction step.

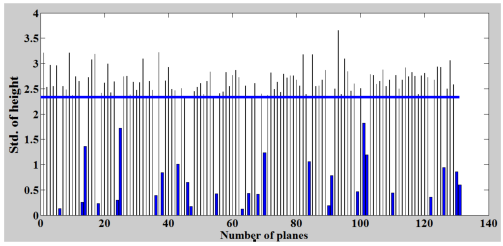

Figure 4: Standard deviation (std.) of height of all the extracted planar segments. Black and blue vertical lines represent std. of height from trees and buildings respectively. The blue horizontal line corresponds to the average std. of height.

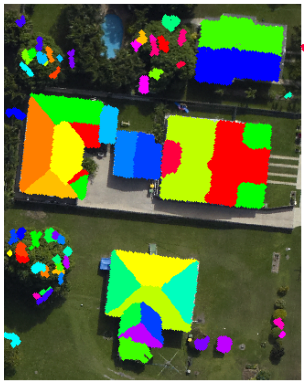

Figure 5: Initial planar segments of a data set marked by different colours and projected on an image.

4.5 A Rule-based Method for Tree Removal

Some of the planes extracted as above may be on trees and other non-building structures such as fence or gutter. To remove those unwanted planes, we propose a rule-based automatic tree removal method. The method defines four rules to remove planar segments on trees. All threshold values use in this method are chosen through a sensitivity analysis.

4.5.1 Plane Neighbourhood Area Ratio: This rule is aimed to remove small planar segments on trees. On a large tree, many small planar segments may be extracted during the initial plane extraction step and they are close to each other but do not form a large plane. For this rule, we choose small planes (area < 5 m^2) and find out their neighbouring planar segments. If a plane has N neighbouring planes and among them N_s are small (area < 5 m^2), the ratio of these two (N_s/N) is considered as a rule to remove planes on trees. If the ratio is more than 60% the planar segment is discarded. This process has the least effect on planar segments over buildings as small planes on buildings may be surrounded by large planar segments. This rule does not consider isolated planes (the plane which has no neighbouring plane) as it can accidentally remove small buildings.

4.5.2 Object Shape Information: The shape information of an object such as *area* and *width* are used to remove planar segments on trees. If a plane has a negligible width ($<= 1$ m) regardless of other parameters the plane is removed. This rule removes the planes that are extracted on the fence or on the gutter. The area of a plane is also considered to remove unwanted planes. For an isolated plane (single plane building) if it has a small area (< 5 m^2) the plane is not considered as a building plane and for non-isolated planes (planes with other big planes in their neighbourhood) the area parameter is reduced to 1 m^2.

4.5.3 Height Gap: To remove trees, the height gap within a plane is calculated. In this measurement, the main concern is for finding any significant height difference in a plane. All of the points in a plane are clustered based on height difference. If there are several clusters, the average height differences for all clusters are calculated. If the average height difference ($>$ 1.5 m proposed in (Awrangjeb et al., 2013)) significantly differs, the plane is considered as a tree plane. The motivation of this observation is, for building plane, there is less height gap as the LiDAR points are continuous in the roof plane. But for the trees, the LiDAR points are coming from various parts of the tree and there may have vertical height gaps in the plane.

4.5.4 Used Point Ratio: The ratio of the used points and actual number of points in a plane is considered as another parameter for tree removal. To calculate the actual number of points, the planar segment is bounded by a rectangular region. All the LiDAR points inside this rectangle are considered as actual points. If the ratio is less than 60%, the plane is marked as tree and removed. Figure 6 shows all the extracted planes after applying the rule-based tree removal method.

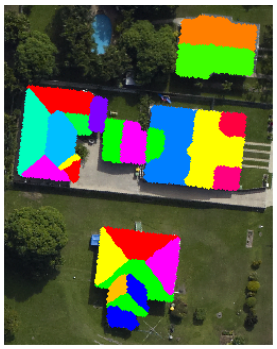

Figure 6: Extracted planar segments after applying a rule-based tree removal method, represented by different colours.

4.6 Building and Plane Boundary Extraction

This is the final step of the method, where the outline of the building is generated. The boundary of the detected buildings and extracted roof planes is shown in Figure 7 for a data set. Images are used only for visualisation purpose.

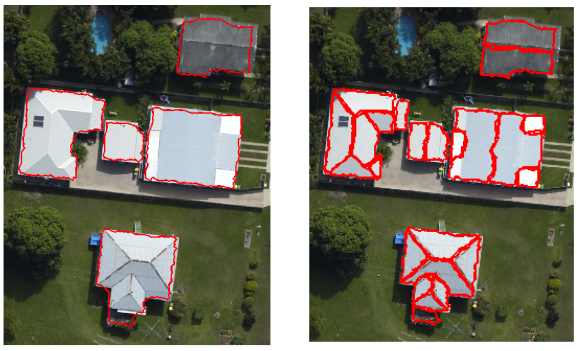

(a) (b)

Figure 7: (a): Detected building boundary; (b): extracted planar segments for a data set.

There are two possible ways for building detection and roof extraction. Some authors (Sampath and Shan, 2010) find out each building and then extract individual roof planes. While the reverse is also possible, where extracted individual roof planes are combined in a neighbourhood basis to detect each building (Awrangjeb and Fraser, 2013). As we extract individual planes so we use the second approach to trace the boundary of each building. For this, the extracted planes are grouped into several clusters based on the Euclidean 2D distance. Each of the clusters represents a building. By combining all the points in a cluster the building outline is obtained. Any building which has an area less than 5 m^2 is removed as per discussion in the previous section. The boundary of the object is determined using a boundary detection approach (Awrangjeb et al., 2012).

5. PERFORMANCE STUDY

5.1 Data Sets

In the conducted performance study six data sets from various states of Australia have been used. Basic information of each data set is provided in Table 1.

Scenes	Full Name	PD	Area	PR
AV1	Aitkenvale Area 1, Qld	40	66 m $\times$ 52 m	F,M
AV2	Aitkenvale Area 2, Qld	29.3	108 m $\times$ 80 m	F,M
HB	Hervey Bay, Qld	12	108 m $\times$ 104 m	F,L
EL	Eltham, Vic	4.8	300 m $\times$ 300 m	H,D
HT	Hobart, Tas	1.6	222 m $\times$ 390 m	H,D
Knox	Knox, Vic	1.2	400 m $\times$ 400 m	H,D

Table 1: Data sets and their basic information. **PD**: point density in points/m^2, **PR**: Properties, **F**: flat area, **H**: hilly area, **L**: low vegetation, **M**: moderate vegetation, **D**: dense vegetation.

The AV1, AV2, and HB data sets are flat in nature with low to moderate vegetation. However, the remaining three data sets have dense vegetation with hilly areas. The point density varies from 1.2 points/m^2 to the maximum 40 points/m^2. Not only the scenes are complex in hilly areas, but they also have low point density. The proposed method is evaluated with the threshold free evaluation approach (Awrangjeb et al., 2010).

5.2 Evaluation Results and Discussion

An evaluation is conducted in pixel-based, object-based, and geometric. Total 13 different metrics are calculated for evaluating building detection results. For roof extraction, 14 metrics are calculated. Seven metrics are used in pixel-based evaluation. In object-based, five metrics are calculated. In geometric-based, two metrics are calculated. Evaluation is also conducted for large buildings and roof planes. Table 2 shows the building detection results for all data sets and Table 3 shows the roof plane extraction results.

Despite of vegetation the completeness and correctness values in pixel-based evaluation are higher than 90% or approximately 90% in AV1, AV2, and HB data sets. Remaining three data sets contain dense vegetation with hilly land structure, though these data sets provide competitive results. The completeness of the Eltham data set is more than 90% with competitive correctness and quality. The proposed method also provides better completeness than correctness and quality in the Hobart data set. Among these three data sets, the evaluation results from the Knox data set are comparatively lower. Most of the buildings of the Knox data set are surrounded by dense trees and some of the buildings are mostly occluded by trees. Due to this, LiDAR points are missed to some parts of the building. In the reference data set, some building parts that are mostly from the veranda are considered as buildings. However, those parts have a few number of

Metrics	AV1	AV2	HB	EL	HT	Knox
C_{pa}	95.2	91.2	96.3	93.2	82	70
CR_{pa}	96.8	92	89.7	76.7	79	86.2
Q_{pa}	92.3	84.5	86.8	72.7	67.4	63
A_{oe}	0.05	0.09	0.04	0.07	0.18	0.3
A_{ce}	0.03	0.08	0.1	0.23	0.21	0.14
B_f	0.03	0.09	0.11	0.3	0.26	0.16
M_f	0.05	0.1	0.04	0.07	0.22	0.43
C_{po}	100	75.4	100	80	65.2	61.5
CR_{po}	100	98	96.3	100	93.7	97
Q_{po}	100	74.2	96.3	80	62.5	60.3
D_{cl}	0.33	0.09	0.08	0.27	0.07	0.1
R_{cl}	0	0	0	0	0.03	0.04
$RMSE$	0.22	0.3	0.32	0.82	0.95	1.40
$C_{po,50}$	100	100	100	100	97.8	97
$CR_{po,50}$	100	98	96.3	100	93.7	97
$Q_{po,50}$	100	98	96.3	100	91.8	94.1
$C_{pa,50}$	95.2	93.4	96.3	94.3	85.2	74.2
$CR_{pa,50}$	96.8	92	89.7	76.7	79	86.2
$Q_{pa,50}$	92.3	86.4	86.8	73.3	69.5	66.3
$A_{oe,50}$	0.05	0.07	0.04	0.06	0.15	0.26
$A_{ce,50}$	0.03	0.08	0.1	0.23	0.21	0.14
$B_{f,50}$	0.03	0.09	0.11	0.3	0.26	0.16
$M_{f,50}$	0.05	0.07	0.04	0.06	0.17	0.35

Table 2: Building detection results. Pixel-based: completeness (C_{pa}), correctness (CR_{pa}), quality (Q_{pa}), area omission error (A_{oe}), area commission error (A_{ce}), branching factor (B_f), and miss factor (M_f) for buildings and buildings over 50 m^2. Object-based: completeness (C_{po}), correctness (CR_{po}), quality (Q_{po}), detection cross lap (D_{cl}), and reference cross lap (R_{cl}) for buildings and buildings over 50 m^2. Geometric: roof mean square error (RMSE).

LiDAR points, so our method cannot detect those buildings. Figure 8 shows the Knox data set along with the detected building boundary which are marked by red colour.

Figure 8: Detected building boundary in the Knox data set.

The area omission error, which represents the percentage of the non-detected building parts is lower than 10% for first three data sets. The area commission error, which represents the percentage of incorrectly detected buildings is also lower than 10% for first three data sets. Branching factor, which measures the degree of over segmentation of buildings non-building parts is also within a reasonable range. The miss factor, which represents the degree

Metrics	AV1	AV2	HB	EL	HT	Knox
C_{pa}	89.6	78.6	85	79.2	69.7	58.9
CR_{pa}	89	77.1	75.1	63.8	63	67.2
Q_{pa}	80.7	63.7	66.3	54.7	49.4	45.7
A_{oe}	0.1	0.21	0.15	0.21	0.3	0.4
A_{ce}	0.11	0.23	0.25	0.36	0.37	0.33
B_f	0.12	0.3	0.33	0.57	0.59	0.49
M_f	0.12	0.27	0.18	0.26	0.43	0.7
C_{po}	96.1	70.3	93.4	79.8	66.5	51.4
CR_{po}	100	92	98.7	82.8	82.2	88.6
Q_{po}	96.1	66.2	92.3	68.5	58.2	48.2
D_{cl}	0.04	0.15	0.06	0.11	0.19	0.28
R_{cl}	0	0.04	0.01	0.12	0.06	0.02
$RMSE$	0.22	0.38	0.38	0.79	0.92	1.16
$RMSE_z$	0.04	0.04	0.08	0.05	0.05	0.05
$C_{po,10}$	100	90.3	99.3	92.6	88.1	71.5
$CR_{po,10}$	100	92	98.7	82.8	82.2	88.6
$Q_{po,10}$	100	83.7	98.1	77.7	74	65.5
$D_{cl,10}$	0.04	0.15	0.06	0.11	0.19	0.28
$R_{cl,10}$	0	0.05	0.01	0.14	0.08	0.03
$C_{pa,10}$	90	81.2	86	81.2	74.7	64.6
$CR_{pa,10}$	89.2	77.1	75.2	63.8	63	67.2
$Q_{pa,10}$	81.1	65.4	67	55.6	51.8	49.1
$A_{oe,10}$	0.1	0.19	0.14	0.19	0.25	0.35
$A_{ce,10}$	0.1	0.23	0.25	0.36	0.37	0.33
$B_{f,10}$	0.12	0.3	0.33	0.57	0.59	0.49
$M_{f,10}$	0.11	0.23	0.16	0.23	0.34	0.55

Table 3: Roof plane extraction results. Pixel-based: completeness (C_{pa}), correctness (CR_{pa}), quality (Q_{pa}), area omission error (A_{oe}), area commission error (A_{ce}), branching factor (B_f), and miss factor (M_f) for roof planes and roof planes over 10 m^2. Object-based: completeness (C_{po}), correctness (CR_{po}), quality (Q_{po}), detection cross lap (D_{cl}), and reference cross lap (R_{cl}) for roof planes and planes over 10 m^2. Geometric: roof mean square error (RMSE) and height accuracy ($RMSE_z$).

of non-detection of a building part, is also within a fair range.

For object-based evaluation, higher results are achieved in AV1 and HB data sets. The correctness has increased in most of the data sets. The completeness is comparatively lower in AV2 data set, since it contains many small buildings or building type objects. Despite of dense vegetation, Eltham data set provides 100% correctness. The correctness of Hobart and Knox data sets are also higher than 90%.

By using only LiDAR data, the accuracy of the boundary is limited to the LiDAR point spacing. For all data sets, the RMSE of the boundary is lower than the respective LiDAR point spacing.

For large buildings, better results are observed in both area-and-object-based. In most of the data sets the completeness is 100% with more than 90% completeness and quality.

The same trend of results is observed in roof extraction as of building detection process. These results are comparatively better in the first three data sets. Despite of dense vegetation, the results from last three data sets are also impressive. Best results are observed for large roof planes. Both the area- and object-based results are improved. Comparatively higher results are found in object-based than area-based. The RMSE is lower than the LiDAR point spacing. The height error is also within a limited range of 8 cm.

Despite of scene complexity and vegetation, our proposed method is able to detect most of the buildings and roof planes. However, some of the buildings and roof planes are missed due to its small size. There are also occlusions from the surrounded trees.

6. COMPARATIVE RESULTS

The outcomes of the building detection and roof plane extraction process are compared with Awrangjeb's method[1]. Here **PM** represents our proposed method and **AW** corresponds to Awrangjeb's method.

Figure 9 shows the object and area-based completeness comparison of building detection process.

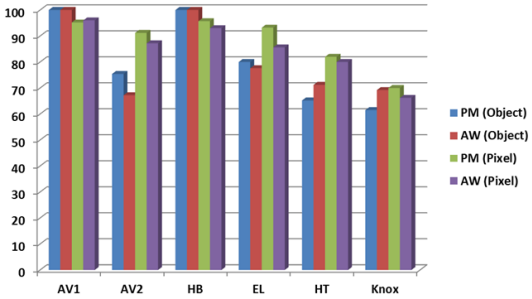

Figure 9: Object and area-based completeness comparison of building detection process. PM (object) and PM (pixel) represent the object and pixel-based completeness of the proposed method. AW (object) and AW (pixel) correspond to the same for Awrangjeb's method. The X-axis labelling represents the data sets.

In object-based evaluation, the proposed method provides better results in all data sets except Hobart and Knox data sets. In our method, we used an updated reference data set where many small sized buildings are included. However, these buildings were not considered in Awrangjeb's reference data set. Despite this, our method outperforms Awrangjeb's method in object-based.

Correctness comparison of these two methods is presented in Figure 10.

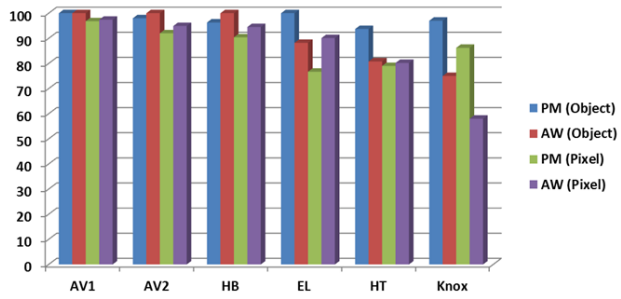

Figure 10: Object and area-based correctness comparison of building detection process. PM (object) and PM (pixel) represent the object and pixel-based completeness of the proposed method. AW (object) and AW (pixel) correspond to the same for Awrangjeb's method. The X-axis labeling represents the data sets.

Despite of the dense vegetation, our proposed method provides better results in Hobart and Knox data sets. The proposed method offers the best result in the Knox data set. For other data sets, both methods provide approximately the same results with an exception in the Eltham data set.

Figure 11 and 12 show the completeness and correctness comparison for roof plane extraction.

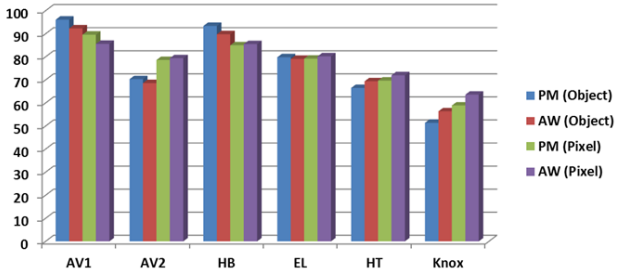

Figure 11: Object and area-based completeness comparison for roof plane extraction process.

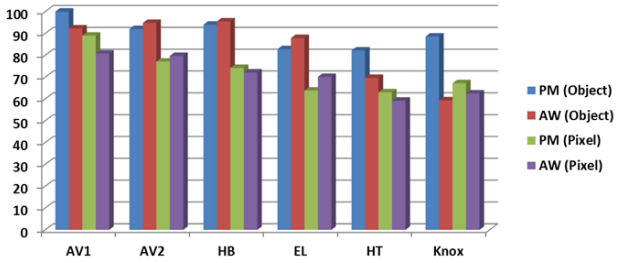

Figure 12: Object and area-based correctness comparison for roof plane extraction process.

For the completeness analysis, our proposed method provides better results in all data sets except in the Knox data set, where the completeness is slightly lower than Awrangjeb's method. An improved performance has been observed in object-based correctness comparison. In the area-based evaluation, both of the methods perform approximately the same.

Figure 13 shows the RMSE of the detected boundary.

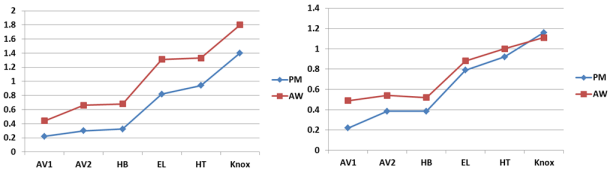

(a) (b)

Figure 13: RMSE comparison of (a): building detection; (b): roof plane extraction. PM: proposed method and AW: Awrangjeb's method

For building detection, our proposed method has significantly lower RMSE than Awrangjeb's method. Therefore the accuracy of the building boundary is much higher in our method. The RMSE of roof plane extraction is also in our favour. However, in the Knox data set Awrangjeb's method provides lower RMSE.

7. CONCLUSIONS

In this paper, we have presented a new automatic LiDAR point segmentation method for building detection and roof plane extraction. Detailed explanation of the proposed method with a

[1] http://users.monash.edu.au/~mawrangj/RExtraction.html

performance study and comparative results were also presented. The method performed well in the presence of vegetation, even in dense vegetation the results were quite impressive. As the method fully depends on the provided LiDAR data, the accuracy of the detection is mostly dependent on the accuracy of the data. There is some future scope of further improvement. The DEM was generated by commercial software. An improved DEM could improve the performance in both building detection and roof plane extraction. The detected boundary can be regularised to generate 3D roof models.

8. ACKNOWLEDGEMENT

The research work presented here has been funded by the Australian Research Council under a Discovery Early Career Researcher Award (Project Number DE120101778). The AV1, AV2 and HB data sets were provided by Ergon Energy (`http://www.ergon.com.au`) in Queensland, Australia. The HT data set was provided by Photomapping Services in Melbourne, Australia. The Knox and EL data sets were provided by the Department of Environment and Primary Industries (`http://www.depi.vic.gov.au/`) of Victoria, Australia.

REFERENCES

Awrangjeb, M. and Fraser, C. S., 2013. Rule-based segmentation of LIDAR point cloud for automatic extraction of building roof planes. In: City Models, Roads and Traffic (CMRT 2013), pp. 1–6. 1, 2, 3, 5

Awrangjeb, M., Ravanbakhsh, M. and Fraser, C. S., 2010. Building detection from multispectral imagery and Lidar data employing a threshold-free evaluation system. In: Photogrammetric Computer Vision (PCV 2010), pp. 49–55. 5

Awrangjeb, M., Zhang, C. and Fraser, C. S., 2012. Building detection in complex scenes thorough effective separation of buildings from trees. Photogrammetric Engineering & Remote Sensing 78(7), pp. 729–745. 1, 2, 3, 5

Awrangjeb, M., Zhang, C. and Fraser, C. S., 2013. Automatic extraction of building roofs using LIDAR data and multispectral imagery. ISPRS Journal of Photogrammetry and Remote Sensing 83, pp. 1–18. 1, 2, 4, 5

Carter, J., Schmid, K., Waters, K., Betzhold, L., Hadley, B., Mataosky, R. and Halleran, J., 2012. Lidar 101: An introduction to lidar technology, data, and applications. NOAA Coastal Services Center. 1

Cheng, L., Gong, J. Y., Chen, X. L. and Han, P., 2008. Building boundary extraction from high resolution imagery and LIDAR data. In: 21st ISPRS Congress, pp. 693–698. 1

Chenga, L., Zhao, W., Han, P., Zhang, W., Shan, J., Liu, Y. and Li, M., 2013. Building region derivation from LiDAR data using a reversed iterative mathematic morphological algorithm. Optics Communications 286, pp. 244–250. 1, 2

Elaksher, A. F. and Bethel, J. S., 2002. Reconstructing 3D buildings from LIDAR data. In: Photogrammetric Computer Vision (PCV 2002), pp. 102–107. 2

Ferro, A., Brunner, D. and Bruzzone, L., 2013. Automatic detection and reconstruction of building radar footprints from single VHR SAR images. IEEE Trans. on Geoscience and Remote Sensing 51(2), pp. 935–952. 1

Habib, A. F., Zhai, R. and Kim, C., 2010. Generation of complex polyhedral building models by integrating stereo-aerial imagery and LIDAR data. Photogrammetric Engineering and Remote Sensing 76(5), pp. 609–623. 1

Kabolizade, M., Ebadi, H. and zadeh, A. M., 2012. Design and implementation of an algorithm for automatic 3D reconstruction of building models using genetic algorithm. International Journal of Applied Earth Observation and Geoinformation 19, pp. 104 – 114. 1

Khoshelham, K. and Li, Z. L., 2005. A split-and-merge technique for automated reconstruction of roof planes. Photogrammetric Engineering and Remote Sensing 71(7), pp. 855–862. 1

Liu, X., 2011. Accuracy assessment of LiDAR elevation data using survey marks. Survey Review 43(319), pp. 80–93. 4

Ma, R., 2005. DEM generation and building detection from lidar data. Photogrammetric engineering and remote sensing 71(7), pp. 847–854. 2

MARS Explorer version 7, 2014. The merrick advanced remote sensing (MARS) software. http://www.merrick.com/Geospatial/Software-Products/MARS-Software. 3

Meng, X., Wang, L. and Currit, N., 2009. Morphology-based building detection from airborne LIDAR data. Photogrammetric Engineering and Remote Sensing 75(4), pp. 437–442. 1, 2

Morgan, M., 2000. Automatic building extraction from airborne laser scanning data. In: 19th ISPRS Congress, pp. 616–623. 3

Noronha, S. and Nevatia, R., 2001. Detection and modeling of buildings from multiple aerial images. IEEE Trans. on Pattern Analysis and Machine Intelligence 23(5), pp. 501–518. 1

Novacheva, A., 2008. Building roof reconstruction from LIDAR data and aerial images through plane extraction and colour edge detection. In: 21st ISPRS Congress, pp. 53–57. 2

Sampath, A. and Shan, J., 2010. Segmentation and reconstruction of polyhedral building roofs from Aerial Lidar point clouds. IEEE Trans. on Geoscience and Remote Sensing 48(3), pp. 1554–1567. 2, 3, 5

Satari., M., Samadzadegan, F., Azizi., A. and Maas, H.-G., 2012. A multi-resolution hybrid approach for building model reconstruction from Lidar data. The Photogrammetric Record 27(139), pp. 330–359. 2

Vu, T. T., Yamazaki, F. and Matsuoka, M., 2009. Multi-scale solution for building extraction from LiDAR and image data. International Journal of Applied Earth Observation and Geoinformation 11(4), pp. 281–289. 1

Wang, J. and Shan, J., 2009. Segmentation of LiDAR point clouds for building extraction. In: ASPRS Annual Conference, pp. 9–13. 2

Zhang, K., Yan, J. and Chen, S. C., 2006. Automatic construction of building footprints from airborne LIDAR data. IEEE Trans. on Geoscience and Remote Sensing 44(9), pp. 2523–2533. 1, 3